Electro-mechanical Modeling of Wind Turbine and Energy Storage Systems with Enhanced Inertial Response

Weihang Yan, Xiao Wang, Wei Gao, and Vahan Gevorgian

***Abstract*—In this paper, a coordinated control scheme for wind turbine generator (WTG) and supercapacitor energy storage system (ESS) is proposed for temporary frequency supports. Inertial control is designed by using generator torque limit considering the security of WTG system, while ESS releases its energy to compensate the sudden active power deficit during the recovery process of turbine rotor. WTG is modeled using the fatigue, aerodynamic, structure, turbulence (FAST) code, which identifies the mechanical loadings of the turbine and addresses electro-mechanical interactions in the wind energy system. A damping controller is augmented to the inertial control to suppress severe mechanical oscillations in the shaft and tower of the turbine during frequency supports. Furthermore, the result of small-signal stability analysis shows that the WTG-ESS tends to improve the stability of the whole multi-energy power grid. The major contributions of this paper will be validated by utilizing the proposed control method that combines the grid support capability and maintaining the integrity of structural design of the turbine for normal operations.**

***Index Terms*—Inertial response, wind turbine generator (WTG), supercapacitor, coordinated control, electro-mechanical transient, structural mode.**

I. Introduction

MOTIVATED by aggressive sustainable energy policies, renewable energy is supplying a large amount of electricity demands in modern power systems. However, the stochastic nature of renewable power makes it difficult to dispatch. The power reserve from conventional power plants might not be enough to accommodate the variations in renewable energy. The majority of commissioned renewable generators operate in grid-following mode, which makes them decoupled from the grid frequency and contribute little to the system inertial response. The low-voltage ride through (LVRT) capability of renewable energy generation units is another concern for reliable grid operations [1]. These issues should be fully addressed before large-scale renewable integrations.

Nowadays, taking wind power plants (WPPs) as an example, they are required to participate in power system frequency regulations in various forms, which is achieved by auxiliary controls beyond basic turbine torque and pitch controls. Modern wind turbine generators (WTGs) are controlled to emulate the behaviors of conventional generators, providing inertial response when under-frequency event happens [2]. In fact, a WTG processes the wider operation range of rotor speed than that of a synchronous generator. Hence, taking advantage of flexible controls of converters, it is possible for WTGs to provide effective frequency regulation to enhance power system stability. Based on these characteristics, some inertial control methods [2], [3] can be added to the power reference of WTG in the power/speed plane by understanding its overloading capability. However, the feasibility of these ideal methods still needs to be examined under turbulent winds for real applications. Deloaded operation is necessary for a turbine to participate in primary frequency and secondary frequency regulations. Power reserve control includes overspeed control and pitch control, but these methods have limitations in full wind regimes. The available power reserved is also distinct for each WTG in a WPP, which further complicates frequency control for system operators.

The advancement of multi-energy system provides undeniable flexibility for power system operation. The distributed energy management problem is solved for multi-energy system in different timescales by designing a novel event-triggered based distributed algorithm [4]. A novel double-mode energy management model is proposed in [5], which unifies the islanded and network-connected modes for multi-energy system. Therefore, a distributed dynamic event-triggered Newton-Raphson algorithm is developed to achieve coordinative operation for all participants with faster convergence rate and better adaptability. Even though various forms of energy have been integrated in multi-energy system, the long-distance energy transmission still relies on electric power net-

Manuscript received: April 30, 2020; accepted: August 20, 2020. Date of CrossCheck: August 20, 2020. Date of online publication: September 26, 2020.

This work was supported by the U. S. National science foundation (No. 1711951). This paper is an extension of the authors' work at National Renewable Energy Laboratory (NREL). The authors sincerely acknowledge the contributions from NREL engineers Andrew Scholbrock, Paul Fleming, and Shahil Shah for providing data and useful discussions during the development of this paper.

W. Yan and W. Gao are with the Department of Electric and Computer Engineering, University of Denver, USA (e-mail: weihang. yan@du. edu; gao18222967451@gmail.com).

X. Wang (corresponding author) is with the Department of Electric and Electron Engineering, The University of Manchester, Manchester, UK (e-mail: xiao. wang-3@manchester.ac.uk).

V. Gevorgian is with the NREL, Golden, USA (e-mail: Vahan. Gevorgian@nrel.gov).

DOI: 10.35833/MPCE.2020.000272

works. As a result, the stability criteria of multi-energy systems still heavily depend on the standard of electric power systems. Within this context, engineers become increasingly aware of the importance of energy storage systems (ESSs) using various energy carriers to make WPP a grid-friendly power plant. ESS technologies for wind power applications have been used for a long time, where ESSs are originally deployed to smooth out the injected WPP power to the grid and enhance the LVRT capability of WPP [6], [7]. Recently, the role of ESS shifts to actively contribute to power system stabilities and improve the ability of WPP in frequency responsive control. The selection of ESS devices depends on power ratings, energy capacities, energy density, and response time. For example, supercapacitor and flywheel are featured by their high power-ramping capabilities, while the battery with high energy density is suitable for long-term frequency control [8].

By combining multi-energy carriers, WTG-ESS formulates a multi-energy generation plant. The mechanical power from the turbine side is transformed to electric power in a more controllable manner. The energy stored or released through supercapacitor enhances the control flexibility of a WTG during system transient state, improves the overall inertial control performance, and relieves mechanical stress on WTG. In this paper, we focus on the coordinated response of the studied system for temporary frequency supports.

References [9] and [10] seek to use the DC-link energy to enhance the inertial response of a WTG. The proposed two methods are similar in principle as the DC voltage dynamics are designed to strengthen the combined inertia constant of WTG-ESS. A cascading control approach is proposed, accounting for the reduced wind energy extraction during frequency response in [9]. Due to the limited capacity of DC capacitor bank, its frequency support is not evident compared with that from rotor kinetic energy (KE). Reference [10] utilizes lithium-ion supercapacitors to improve the energy capacity of the DC bank of a Type III WTG, then a desirable inertial control can be achieved. The sizing, cost, and weight of the supercapacitor are discussed for the combined inertial response in WTG. References [11] - [14] coordinate the actions of WTG and ESS with complex control logics, where releasable KE in the turbine rotor, storage state of charge (SOC), and the grid frequency profiles are considered. ESS is primarily used to suppress the secondary frequency dip (SFD) caused by rotor KE restoration in [11], [12]. The power reference of ESS is determined by the sudden deloading action in WTG inertial control using torque limit [11]. Knowledge-based methods are also widely employed to achieve optimal WTG and ESS operations. The fuzzy-logic based controller is mentioned in [13] and [14], where the WTG-ESS is designed to provide multi-timescale frequency response using a state-machine based controller.

In order to maximize the contribution of WTG in frequency regulation, we design the inertial control scheme for WTG based on the generator torque limit which is similar to the concepts presented in [11], [15]. A deficiency identified with this method is that the deloaded operation is activated when the rotor speed settles at a quasi-steady state, which is difficult to be detected with turbulent winds. Furthermore, we intend to address the factors that are potentially damaging to a WTG and propose modifications considering system safety. References [11] and [16] adopt more straightforward torque-limit-based inertial control (TLIC) methods by commanding the generator torque at its limit during the whole process of inertial response. It points out that this method would be beneficial to the independent system operator (ISO) since the available power increase can be predicted [16]. The same control concept is employed in [11] with the coordination from the battery ESS. However, the duration is ignored when the torque is operated at its limit. The generator torque limit is also related to the current limit of the power switches (overloading capability of RSC), therefore, its duration should be restricted to avoid permanent thermal breakdown of the power electronic devices. The start of the deloaded action is decided by the pre-disturbance WTG power output and grid frequency rebound, before which the power converters could be damaged as long-term overcurrent is initialized. The same issue will also occur in the region with high wind speed, especially for that considered in [15]. The torque limit provides headroom for power increase under the rated condition. As the active power reference is designed to decrease with rotor speed, WTG may get trapped in the torque limit point with invariant rotor speed controlled by the pitch. Therefore, long-term overload could sustain until the wind speed decreases.

From the perspective of mechanical structure of the turbine, efforts are made to improve the controller's performance in damping the structural modes of flexible wind turbines (WTs) [17]. Some studies utilize the model of wind power system based on the fatigue, aerodynamic, structure, turbulence (FAST) of turbine simulator, thus the interactions between mechanical and electrical systems of the turbine can be observed in simulations [18], [19]. Reference [14] presents that a voltage sag at point of common coupling (PCC) may trigger severe oscillations of turbine tower. Cyclical mechanical loadings induced by blade rotation can also affect the power qualities in an isolated grid [7], [19]. Results in [20], [21] and [22] reveal that active power controls of the turbine tends to increase mechanical burdens on the drivetrain, while the thrust-related loadings can be reduced in this process. In this paper, we further highlight the electro-mechanical transients of the turbine system during inertial controls with multi-energy participations. We propose a damping method to mitigate the mechanical loading escalation at the turbine shaft and tower when the inertial control is activated.

To perform these tasks, we first introduce the modeling of wind power system with the FAST program. Using real aerodynamics and airfoil data measured in field tests, the model is developed for a 3-bladed controls advanced research turbine (CART3) located at the Flatirons Campus, National Renewable Energy Laboratory (NREL) (National Wind Technology Center) in Colorado, USA. The control of rotor-side converter (RSC) and grid-side converter (GSC) is synthesized systematically, based on which the auxiliary control is designed. The supercapacitor is connected directly at the DC link, solving the SFD caused by KE restoration. Finally, the coordinated response of the studied system is verified based

on the CART3 model integrated in the IEEE 14-bus test system. Small-signal studies are carried out to prove the improved inertial response from the perspective of the whole multi-energy network.

The rest of this paper is organized as follows: Section II illustrates the proposed CART3-PMSG simulation model. In Section III, the control of power converters is presented, and the coordinated control scheme with damped structural modes is elaborated in Section IV. Case studies are presented in Section V and the paper is finalized in Section VI.

II. Modeling of CART3-PMSG System

CART3 employs a Type IV WTG configuration with full power converters. The mechanical system is modeled on the FAST simulation platform by considering the dynamics in the turbine shaft, blades, and tower. The permanent-magnetic synchronous generator (PMSG) is represented by its voltage and flux equations in rotating reference frame. An overview of the simulated system is given in Fig. 1. The signals of rotating speed and mechanical torque on the high-speed shaft (HSS) is fed from FAST to PMSG model, and the electromagnetic torque is an external input to FAST.

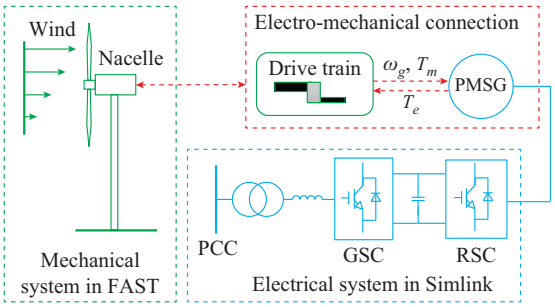

Fig. 1. A comprehensive wind energy system modeling based on FAST.

A. Modeling of WTG Mechanical System in FAST

FAST is a high-fidelity aeroelastic turbine simulator developed by the NREL [23]. It can be used to simulate horizontal-axis WTs with two or three blades. Based on the combined modal and the formulation of multibody dynamics, at most 24 degree of freedoms (DOFs) can be selected to predict the behavior of WTs [24]. In addition to the shaft DOFs, the dynamics in the turbine tower and blades are proven to have evident impacts on turbine operations with increased structural flexibility. These DOFs are shown in Fig. 2.

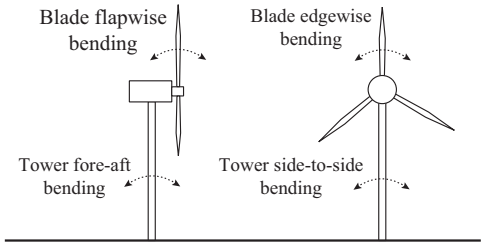

Fig. 2. Interested DOFs in turbine tower and blades.

The motion equations of DOFs are set up using Euler-Lagrange method in FAST as denoted in (1), which is solved by numerical integrations.

$$\boldsymbol{M}(\boldsymbol{q},\boldsymbol{u},t)\ddot{\boldsymbol{q}}+\boldsymbol{f}(\boldsymbol{q},\dot{\boldsymbol{q}},\boldsymbol{u},\boldsymbol{u}_d,t)=\boldsymbol{0} \tag{1}$$

where $\boldsymbol{M}$ is the mass matrix of considered components; $\boldsymbol{q},\dot{\boldsymbol{q}},\ddot{\boldsymbol{q}}$ are the displacements, velocities and accelerations of selected DOFs, respectively; and $\boldsymbol{u}$ and $\boldsymbol{u}_d$ are the control and disturbance inputs, respectively. The dynamic motions given in (1) are driven by the induced aerodynamic forces $\boldsymbol{f}$, which is calculated by the subroutine AeroDyn embedded in the FAST code. The inputs to AeroDyn include full-field wind speed, geometrical data of blades and motion information of DOFs. The calculated forces are returned as feedbacks to the FAST code for the evaluation of the structure dynamics in the next step.

In this paper, the FAST code is used to model a 600 kW modern turbine CART3 equipped with various sensors to monitor its operation and performance in field. CART3 and its corresponding power coefficient are shown in Fig. 3, where the photo is provided by Andrew Scholbrock. These data are recorded during the rotor commission based on proper procedures. Other parameters for the mechanical system of CART3 are listed in Table AI in Appendix A. The selected DOFs are variable-speed generator DOF, shaft torsional DOF, flapwise blade bending DOF, and the tower side-to-side bending DOF in FAST.

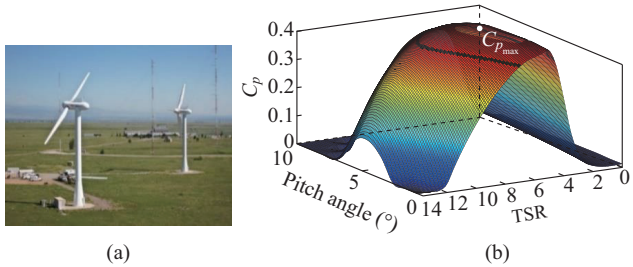

(a) (b)

Fig. 3. CART3 and its power surface. (a) CART2 (left) and CART3 (right). (b) CART3 C_p.

B. Modeling of WTG Electrical System in Simulink

A low-speed PMSG is usually built with multiple poles, thus it can be directly driven by the low-speed shaft (LSS) without a gearbox. Such a compact WTG structure leads to high reliability, which is always adopted in scenarios requiring considerable maintenance cost such as offshore wind applications. Permanent magnet is employed for the flux generation, and the dynamic model of a PMSG is formulated as in (2)-(4).

$$\frac{\mathrm{d}}{\mathrm{d}t}\begin{bmatrix}\lambda_{sd}\\ \lambda_{sq}\end{bmatrix}=\begin{bmatrix}0 & \omega_g\\ -\omega_g & 0\end{bmatrix}\begin{bmatrix}\lambda_{sd}\\ \lambda_{sq}\end{bmatrix}+\begin{bmatrix}-R_s & 0\\ 0 & -R_s\end{bmatrix}\begin{bmatrix}i_{sd}\\ i_{sq}\end{bmatrix}+\begin{bmatrix}v_{sd}\\ v_{sq}\end{bmatrix} \tag{2}$$

$$\begin{bmatrix}\lambda_{sd}\\ \lambda_{sq}\end{bmatrix}=\begin{bmatrix}L_d & 0\\ 0 & L_q\end{bmatrix}\begin{bmatrix}i_{sd}\\ i_{sq}\end{bmatrix}+\begin{bmatrix}\lambda_m\\ 0\end{bmatrix} \tag{3}$$

$$T_e=\frac{3}{2}(L_d-L_q)i_{sd}i_{sq}+\frac{3}{2}\lambda_m i_{sq} \tag{4}$$

where λ_{sd} and λ_{sq} are the stator fluxes in dq frame; λ_m is the rotor flux; ω_g is the rotating speed of the high-speed turbine shaft; R_s is the stator resistance; L_d and L_q are the stator in-

ductances in *dq* frame; v_{sd}, v_{sq}, i_{sd}, and i_{sq} are the stator voltages and currents in *dq* frame, respectively; and T_e is the electromagnetic torque of PMSG. These equations are represented in *dq* frame aligned to the rotor position. Other electrical components in the WTG system are simulated in MATLAB/Simulink using average models. Detailed PMSG parameters are shown in Table AII of Appendix A.

III. Control of Power Converters

Three control units working in coordinative manner are presented to achieve the desired wind power extraction. The pitch control and RSC control mainly deal with rotor speed regulations, and the GSC stabilizes the DC-link voltage and regulates reactive power injection to the grid. A gain-scheduling PI control is employed for blade pitch regulations in CART3. The detailed description can be found in [24]. The RSC and GSC manipulate the stator currents of PMSG and grid-side current injection. This section mainly describes a systemic design for power converter control.

A. RSC Control

RSC regulates T_e based on the vector control concept. According to (4), i_{sd} is usually controlled to zero due to the insignificant rotor saliency, thus T_e can be solely determined by stator current on *q*-axis i_{sq}. To control the stator current on *d*-axis i_{sd} and i_{sq}, (3) is substituted into (2) to formulate current dynamics in *dq* frame, as in (5) and (6).

$$L_d \frac{\mathrm{d}i_{sd}}{\mathrm{d}t} = -R_s i_{sd} + u_{d,rsc} \tag{5}$$

$$L_q \frac{\mathrm{d}i_{sq}}{\mathrm{d}t} = -R_s i_{sq} + u_{q,rsc} \tag{6}$$

where the control variables $u_{d,rsc}$ and $u_{q,rsc}$ are assigned as:

$$u_{d,rsc} = L_q \omega_g i_{sq} + v_{sd} \tag{7}$$

$$u_{q,rsc} = -L_d \omega_g i_{sd} - \lambda_m \omega_g + v_{sq} \tag{8}$$

With compensators having PI control forms, transfer functions of the PI controllers for the RSC can be derived as following.

$$k_{d,rsc}(s) = \frac{L_d s + R_s}{\tau_{rsc} s} \tag{9}$$

$$k_{q,rsc}(s) = \frac{L_q s + R_s}{\tau_{rsc} s} \tag{10}$$

where τ_{rsc} is the time constant of the current loop of RSC.

Hence, combining (5), (6) and (9), (10) in Laplace domain, the closed-loop systems become first order transfer function with τ_{rsc}, as in (11).

$$\frac{I_{sd}(s)}{I_{sd,ref}(s)} = \frac{I_{sq}(s)}{I_{sq,ref}(s)} = \frac{1}{1+\tau_{rsc} s} \tag{11}$$

where $I_{sd}(s)$, $I_{sq}(s)$, $I_{sd,ref}(s)$, and $I_{sq,ref}(s)$ are the current injections of GSC and their references in the Laplace domain, respectively. The control inputs to RSC are voltage references $v_{s,abc}$ at the stator terminal of PMSG as determined through (7) and (8).

B. GSC Control

GSC is regarded as a DC-voltage port for controller development, whose core is the active/reactive power controller that manipulates power exchanges at PCC [25]. With the inner current control loops nested inside the outer loop that controls the DC voltage, the controlled DC-voltage port has a cascading control structure. Once the DC voltage is imposed as constant, the power generated from the RSC side is consistently and smoothly transferred to the GSC side and injected into the grid. The controller analysis is presented in the *dq* frame synchronized to the grid voltage [26]. The current dynamics i_d and i_q of the RL filter are expressed as in (12) and (13).

$$L \frac{\mathrm{d}i_d}{\mathrm{d}t} = L\omega_0 i_q - R i_d + v_{td} - v_{gd} \tag{12}$$

$$L \frac{\mathrm{d}i_q}{\mathrm{d}t} = -L\omega_0 i_d - R i_q + v_{tq} - v_{gq} \tag{13}$$

where R and L are the resistance and inductance of the RL filter, respectively; ω_0 is the grid frequency in angular speed; and v_{td}, v_{tq}, v_{gd}, and v_{gq} are the turbine terminal voltages and grid voltages in *dq* frame, respectively. The current references of GSC, $i_{d,ref}$ and $i_{q,ref}$, can be calculated from the power references $P_{s,ref}$ and $Q_{s,ref}$:

$$i_{d,ref} = \frac{2}{3v_{gd}} P_{s,ref} \tag{14}$$

$$i_{q,ref} = -\frac{2}{3v_{gd}} Q_{s,ref} \tag{15}$$

Similar to RSC control, we define control variables $u_{d,gsc}$ and $u_{q,gsc}$ for GSC control. Substituting them into (12) and (13), we can obtain:

$$L \frac{\mathrm{d}i_d}{\mathrm{d}t} = -R i_d + u_{d,gsc} \tag{16}$$

$$L \frac{\mathrm{d}i_q}{\mathrm{d}t} = -R i_q + u_{q,gsc} \tag{17}$$

Similarly, with PI compensators, the transfer functions of GSC current controllers in (18) can be derived as follows, where τ_{gsc} is the designed time constant of the current loop of GSC.

$$k_{d,gsc}(s) = k_{q,gsc}(s) = \frac{Ls + R}{\tau_{gsc} s} \tag{18}$$

The closed-loop GSC current dynamics $G_i(s)$ are identical for the *d* and *q* current components as:

$$G_i(s) = \frac{I_d(s)}{I_{d,ref}(s)} = \frac{I_q(s)}{I_{q,ref}(s)} = \frac{1}{1+\tau_{gsc} s} \tag{19}$$

Again, the voltage references v_{td} and v_{tq} for controlling the converter can be obtained through (12) and (13).

In the outer control loop, the compensator controls the DC voltage V_{dc} by regulating active power P_s and reactive power Q_s delivered to PCC. The system dynamics that link the control variable P_s and V_{dc} is described in (20) [25].

$$\frac{\mathrm{d}\tilde{V}_{dc}^2}{\mathrm{d}t} = \frac{2}{C}\tilde{P}_{ext} - \frac{2}{C}\left(\tilde{P}_s + \frac{2LP_{s0}}{3v_{gd}^2}\frac{\mathrm{d}\tilde{P}_s}{\mathrm{d}t}\right) + \frac{2}{C}\frac{2LQ_{s0}}{3v_{gd}^2}\frac{\mathrm{d}\tilde{Q}_s}{\mathrm{d}t} \tag{20}$$

where P_{ext} is the active power imposed on DC link from turbine side; C is the capacitance of DC side; the superscript ~ denotes small-signal perturbations under the steady-state condition; and the subscript 0 in variables denotes the equilibrium, e.g., P_{s0} is the steady-state power injection of GSC, $\tilde{P}_s$ is the deviations from this operation point, and Q_{s0} is the reactive power of GSC. Then, (20) is transformed into Laplace domain as in (21) to derive DC voltage controller $G_v(s)$.

$$G_v(s)=\frac{\tilde{V}_{dc}^2(s)}{\tilde{P}_s(s)}=-\frac{2}{C}\frac{\tau s+1}{s} \tag{21}$$

$$\tau=\frac{2LP_{s0}}{3v_{gd}^2}=\frac{2LP_{ext0}}{3v_{gd}^2} \tag{22}$$

where P_{ext0} is the steady-state active power delivered to DC side from RSC. Note that τ is determined by P_{ext0}. A negative τ results in a non-minimum phase system, leading to a reduction in the phase of $G_v(s)$. This phase lag should be accounted for in the compensator design to ensure sufficient system phase margin [25]. In a Type III wind power system, the power flow is bidirectional through the power converters. P_{ext0} is negative in the sub-synchronous mode when the generator operates at the speed below the synchronous speed. The power flow is unidirectional from generator stators to the grid in most cases in a Type IV wind power system. However, because an ESS is connected at the DC link for enhanced inertial response, the power needs to be absorbed from the grid to charge the ESS. The importance of a lead compensator should be emphasized to ensure the stability of the WTG-ESS system. The DC voltage compensator $K_v(s)$ consists of a lead term $N(s)$ and an integral term as:

$$K_v(s)=-\frac{N(s)}{s} \tag{23}$$

The open loop transfer function of GSC side $L(s)$ is obtained by including dynamics of the GSC current control loops:

$$L(s)=K_v(s)G_v(s)G_i(s)=N(s)\frac{2}{C}\frac{\tau s+1}{s^2(\tau_{gsc}s+1)}=N(s)G(s) \tag{24}$$

A useful formation for the lead compensator is denoted as:

$$N(s)=\frac{\sqrt{b}}{|G(j\omega_c)|}\frac{s+\omega_c/\sqrt{b}}{s+\omega_c\sqrt{b}} \tag{25}$$

At ω_c, an approximate 75° phase margin is achieved with $b=20$. Detailed control parameters of power converters are shown in Table AIII in Appendix A.

IV. Coordinated Control Strategies

The proposed coordinated control strategy is presented in this section. The turbine inertial response is developed based on the torque limit (1.2 p.u.), and the supercapacitor is used to avoid SFD caused by deloaded operation. The supercapacitor is deployed directly at the DC link of WTG, thus GSC can be used to perform charging/discharging controls for ESS. A damping controller is added in the torque control loop to suppress severe shaft and tower oscillations due to inertial response. The sizing of the supercapacitor is also discussed based on the prior simulations.

A. Inertial Response Considering WTG System Security

In this sub-section, we propose a modified TLIC method considering the potential issues of original methods discussed in Section I. The methods are based on our practical experience that is obtained when TLIC method is firstly implemented on CART3. The TLIC method is modified by considering the security of WTG system as described in Fig. 4, with the power reference P_{TLIC} denoted as in (26).

$$P_{TLIC}=\begin{cases}T_{lim}\omega_g & \omega_0/(2\pi)<59.8\\ K_g\omega_g^3 & \omega_g<\omega_{g,\min}\ \text{or}\ t_{BC}>t_0\end{cases} \tag{26}$$

where T_{lim} is the turbine torque limit; and K_g is the maximum power point tracking (MPPT) coefficient. WTG provides a timely power surge by switching the operation point from A to B once the frequency event is detected. The deloading (C→D) is activated when the prescribed overproduction duration t_0 is attained or when the rotor speed decreases down to the minimum value. Considering the overproduction capability of the CART3 system, t_0 is set to be 5 s, which means that the turbine will terminate the frequency support after 5 s and switch back to MPPT operation.

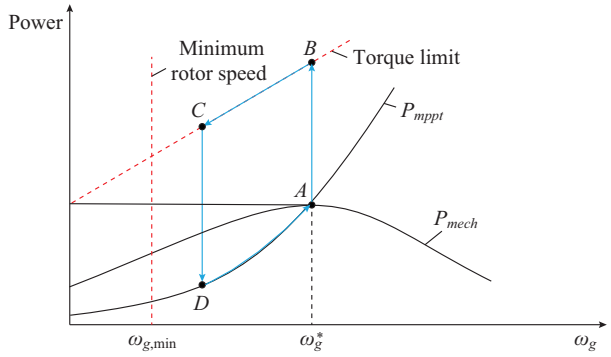

Fig. 4. Active power reference for modified TLIC method.

B. Coordinated Actions with Supercapacitor

The proposed TLIC ensures the reliability of the WTG system, and it is effective in real applications without complex control logics. However, the sudden active power deficit is relatively large when the deloading starts. Such power difference ΔP_{de} is given as:

$$\Delta P_{de}=T_{lim}\omega_g-K_g\omega_g^3 \tag{27}$$

The extreme value is obtained by setting the derivate of (27) to be zero, e.g., the maximum power decrease could be 282.44 kW when the deloading operation happens at the generator speed of 120.21 rad/s. If the active power deficit is not balanced by the DC-link energy, deteriorated SFD could occur. As presented in Section III-B, GSC cascading control structure is the basis for DC energy release. Auxiliary controls are designed to mitigate SFD using a power-rate limiter at the GSC side. The control logics are given in Fig. 5.

A sudden decrease in T_e happens when the deloading starts, which will enable the DC-side voltage auxiliary control. The power-rate limiter restricts sudden power decrease by setting the allowable power change rate between ($-P_{r,\min}$,

$+\infty$) at the GSC side. Due to the power-rate limit, active power difference between the RSC side and GSC side should be compensated by the energy storage. The released DC-side energy E_{rel} is governed by energy equation in (28).

$$E_{rel}=\frac{1}{2}C_{sup}(V_{dc}^2-V_{dc0}^2-\Delta V_{dc}^2)=\int(P_s-\omega_g T_e)\mathrm{d}t \tag{28}$$

where C_{sup} is the capacitance value of the supercapacitor.

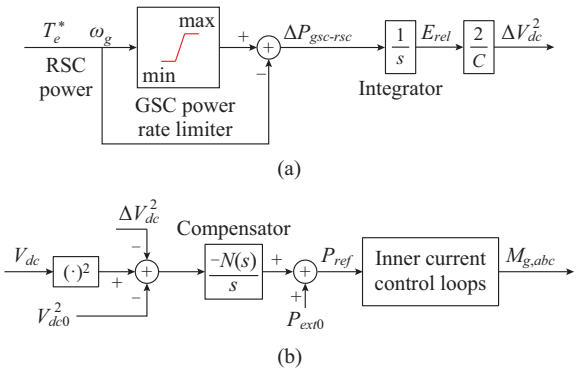

Fig. 5. Diagram of DC-link auxiliary control for mitigating SFD. (a) DC voltage auxiliary control. (b) GSC cascaded controls.

In this paper, the model of supercapacitor is referred in [27] and [28]. Since V_{dc} is controlled as a constant before the disturbance, the squared change of DC voltage can be simply determined by the released energy from supercapacitor, as in (29).

$$\Delta V_{dc}^2=2E_{rel}/C_{sup} \tag{29}$$

The calculated ΔV_{dc}^2 will be added to the voltage control loop, thus the energy stored in DC-side supercapacitor is released, and the power decrease rate at PCC is restricted to prevent obvious impacts on grid frequency. As the turbine gradually accelerates to the pre-disturbed speed, ΔV_{dc}^2 decreases to zero, and the supercapacitor stops participating in the frequency support of WTG.

C. Sizing of Supercapacitor

The sizing of the supercapacitor is determined by prior simulations. Based on the developed CART3-PMSG model, we set up a series of simulations with different wind speeds and different GSC power-rate limits. ΔV_{dc}^2 is not added to the DC voltage controls, but the required energy is calculated during such process. The simulation results are shown with the interpolation in Fig. 6.

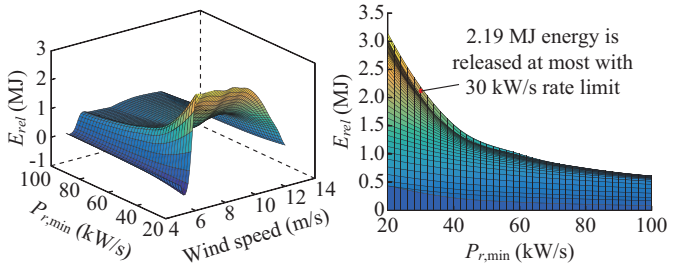

Fig. 6. Required energy from the DC link with respect to different wind speeds and GSC power-rate limiters. (a) 3-dimentional plot. (b) Side view of 3-dimentional plot.

As expected, there is an increase in the demand of DC-link energy as the absolute values of GSC power-rate limits decrease. Compared with the required energy in low and high wind speed regions, the required energy is higher in middle wind speed region due to the larger deloaded power.

The sizing of the supercapacitor should ensure that the DC voltage is still within allowable range for stable operations of the power converters when the maximum energy is released. In this paper, the GSC power-rate limit is selected as 30 kW/s to reduce SFD as much as possible. Normally, this value should be selected considering the power-ramping capabilities of conventional generators in different power grids. A small power-rate limit (absolute value) can significantly mitigate SFD, but this will lead to an increase in the energy requirement and sizing of the supercapacitor. With this power-rate limit, the maximum required energy is 2.19 MJ as shown in Fig. 6. If the supercapacitor is selected as 1 F, then the DC voltage will reduce to 2150 V when such amount of energy is released. According to [25], the allowable DC voltage is determined by (30), which has been simplified considering unity power factors for GSC operation.

$$V_{dc}\geq 2\sqrt{v_{td}^2+v_{tq}^2}=2\sqrt{v_{gd}^2+\left(\frac{2L}{3\tau_{GSC}v_{gd}}\Delta P_s\right)^2+\left(\frac{2L\omega_0}{3v_{gd}}P_{s0}\right)^2} \tag{30}$$

It indicates that the possible minimum DC voltage is collaboratively determined by the steady-state active power P_{s0}, and the sudden power change ΔP_s in the worst-case scenario. ΔP_s is set to be 283 kW as identified in (27) under the extreme conditions. P_{s0} is selected as the rated power of CART3. As calculated, V_{dc} should be larger than 962 V to ensure the stability. Thus, there exists enough voltage margin for stable system operation.

D. Damping of Turbine Shaft and Tower Mode

The inertial control design is based on WTG torque limit that draws extensive attentions recently [11], [15], [16]. However, none of these studies examine the change of mechanical loadings of the turbine by extracting KE with such aggressive torque commands. The inertial response tends to increase the shaft torque and tower side-to-side movement. Commonly, the change rate of generator torque is limited to prevent extreme loadings on turbine shaft, but this will slow down the inertial response of the turbine in frequency support. In this paper, a state-feedback controller is designed to damp the structural oscillations. This is an important contribution of this paper, since the proposed controller must be effective without threatening the integrity of structural design of the WT for normal operations.

The nonlinear motion in (1) is linearized for the following controller synthesis. We only consider the shaft and tower DOFs because the controller is mainly designed to damp the oscillations in these components. In the general linear state-space model of the mechanical part of the turbine, the system states are selected following the FAST convention [19], as $\boldsymbol{x}=[q_4, q_{tw}, q_8, \dot{q}_4, \dot{q}_{tw}, \dot{q}_8]^{\mathrm{T}}$, where q_4 is the rotor azimuth angle; $q_{tw}=q_4-q_{15}$ are the drive-drain torsional angle; q_{15} is

the HSS azimuth angle converted to the LSS; and q_8 is the tower side-to-side displacement.

HSS speed and tower side-to-side displacement are measured in the system output. The system matrices are computed by FAST through numerical approach. The states consist of selected DOFs and their derivatives, which are represented in terms of small deflections around the operation points. The controller is realized in the generator torque control loop as shown in Fig. 7. The damping controller generates the damping torque ΔT and adds to T_{lim}. The torque limit is de-rated to 1.18 p.u. compared with the original 1.2 p.u. on CART3.

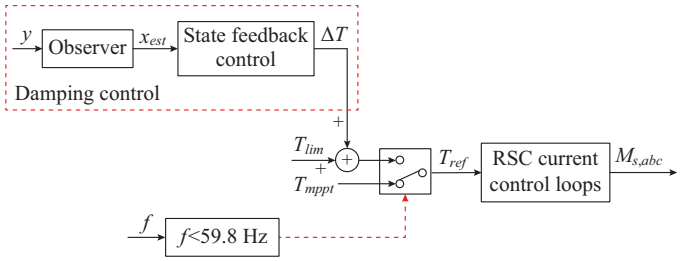

Fig. 7. Modified RSC torque control with additional damping functions.

The mechanical system of the turbine is linearized around the operation point that has 10 m/s wind speed, under which the system open-loop poles are (−0.0394, −0.0942±1.113i, −0.0041±5.554i). It corresponds to the generator speed mode, drive-train torsional mode, and tower side-to-side bending mode, respectively. The state feedback gain is designed to place the closed-loop poles at (−0.0394, −1±18.113i, −0.05± 5.554i), hence, significant damping is added to the shaft and tower modes. A state observer is included to estimate the system states.

V. Case Studies

A. Simulation Setups

CART3-PMSG is aggregated into a WPP with 100 identical WTs. As shown in Fig. 8, WPP is connected at bus 14 of the modified IEEE 14-bus test system. The model of IEEE 14-bus test system is based on [29] and [30] and simulated in MATLAB/Simulink. Key parameters of the test system are listed in Table A IV in Appendix A. Five synchronous generators and one WPP supply 575 MW loads in total. The nominal frequency is 60 Hz. Each synchronous generator is equipped with a governor and an excitation control. The droop coefficient is set to be 20% in this test grid. The synchronous generator at bus 2 is intentionally tripped to trigger the under-frequency event. The case studies are carried out under turbulent winds generated by TurbSim, which is a full-field wind speed simulator developed by NREL [31]. The mean wind speeds at the hub height are set to be 7 m/s, 10 m/s, 18 m/s with 10% turbulence intensity, corresponding to the low, middle, and high wind speed regions, respectively. A vertical power law shear component is included in the wind speed data to excite structural modes of the turbine [31]. The power law exponent is set to be 0.2 in the simulations.

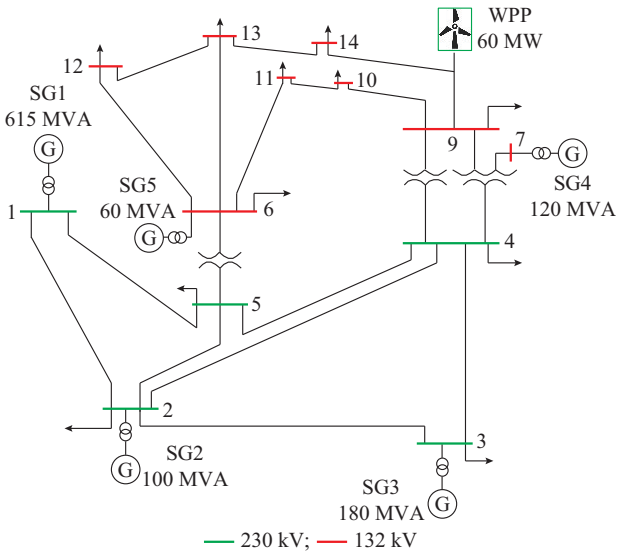

Fig. 8. CART3-based WPP connected into IEEE 14-bus test system.

As mentioned in Section III, the voltage control loop of the GSC is essential to coordinate the energy stored in the supercapacitor. The power can be extracted from the PCC to the DC side, a lead term should be included to solve the non-minimum phase problem by the voltage controller. Based on the parameters in Table AIII, the compensator (23) is tuned at 200 rad/s, which is one fifth of the time constant of current control loops.

B. Response of WTG-ESS System

In Figs. 9 and 10, we evaluate the proposed coordinated control scheme (red line) as well as TLIC without supercapacitor's support (green line), the TLIC with torque-rate limit (blue line), and the baseline without inertial response (black line). The torque-rate limit is effective to restrict sudden torque changes on the shaft, but the inertial response would be slowed. The generator torque-rate limit is set to be 0.45 p.u./s [15].

Generally, the results presented in Figs. 9 and 10 are used to demonstrate the effectiveness of the proposed method. Obviously, the proposed inertial control not only improves the trajectory of power system frequency after generator tripping, but also provides better oscillation damping on turbine mechanical components which is excited by the increasing aggressive torque. Compared with the baseline without turbine inertial response, the proposed method obviously improves the frequency nadir (FN) by delivering additional power for grid support. Comparing the proposed method with original TLIC without storage, SFD can be observed when the turbine deloading is enabled. Regarding the mechanical parts of the turbine, the proposed method provides additional damping on the turbine shaft and tower. Since a torque rate limit is usually used to mitigate the impacts of sudden torque change in real turbine system, we also compare the proposed method with TLIC using such a torque rate limit. The result indicates that the torque rate limit is effective to reduce structure oscillations but yields a deteriorated frequency support due to the slowed response.

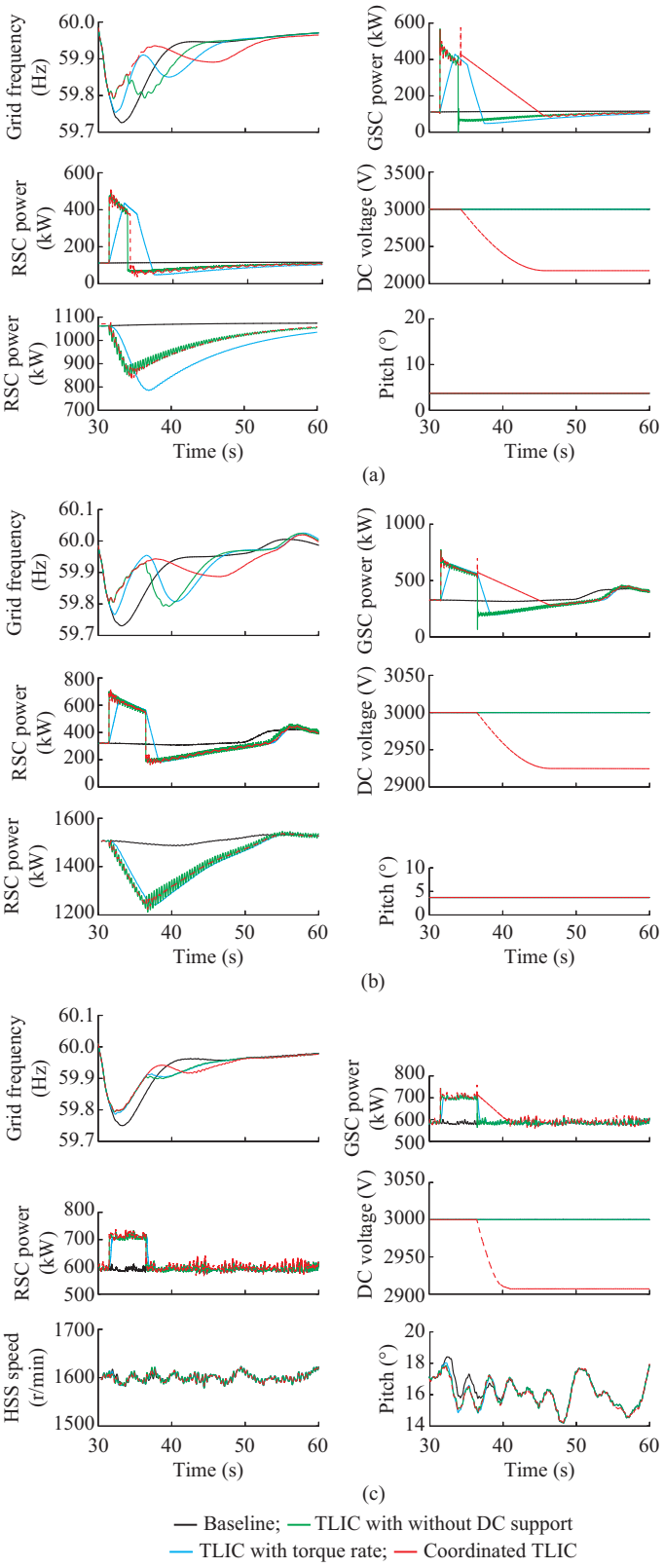

Fig. 9. Performance comparison of WTG frequency support using different inertial control algorithms. (a) 7 m/s. (b) 10 m/s. (c) 18 m/s.

1) Inertial Response Evaluated with Turbulent Wind Speeds

The simulation resulting in the low wind speed region are illustrated in Fig. 9(a). It shows that the frequency support is terminated as the rotor speed hits the lower speed limit (850 r/min), which prevents the system from shutting down. From the system frequency profile under both low wind (Fig. 9(a)) and medium wind conditions (Fig. 9(b)), the TLIC method improves the FN significantly compared with the baseline without inertial response and TLIC with torque-rate limit.

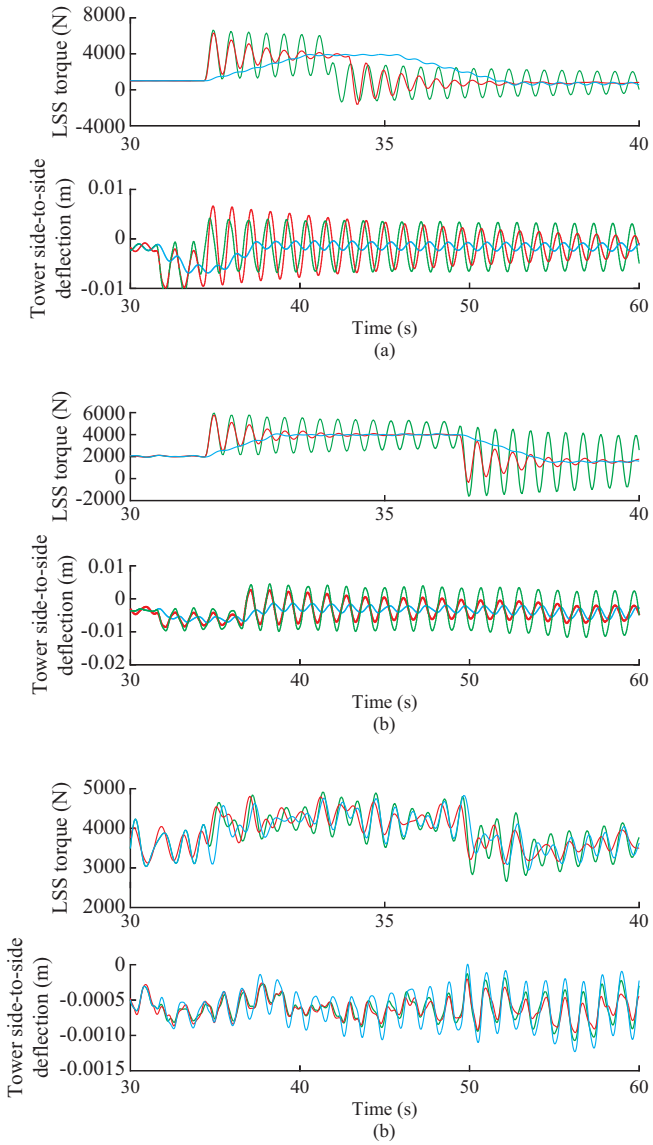

Fig. 10. Effects of augmented damping controller in inertial controls with hub-height mean wind speeds. (a) 7 m/s. (b) 10 m/s. (c) 18 m/s.

However, without the support from DC-link supercapacitor, significant SFD is observed in the original TLIC method during KE recovery process.

With the proposed coordinated approach, active power support from DC link is activated when the deloading operation starts. The active power output at the GSC side gradually decreases to pre-disturbed level with the power injection from the storage at DC side. The energy released from supercapacitor becomes zero when WTG reaches pre-disturbed condition, and DC-link voltage is stabilized at a lower level than its nominal value. The generator speed has already shown some oscillations using TLIC without enabling DC-side support. This is because no damping control is added to

this TLIC method.

In TLIC with torque-rate limit, the generator speed is lower than the minimum value due to the slow torque response, which potentially affects the reliability of the turbine system. The effectiveness of the proposed coordinated control scheme is more evident in the middle wind speed region as shown in Fig. 11(b). The proposed method presents an improved FN compared with the case of TLIC with torque-rate limit and the baseline. WTG is operated at torque limit for predefined duration considering the rated power of converter. With the coordinated action from the supercapacitor, SFD is lower than the case without coordination when the deloading happens.

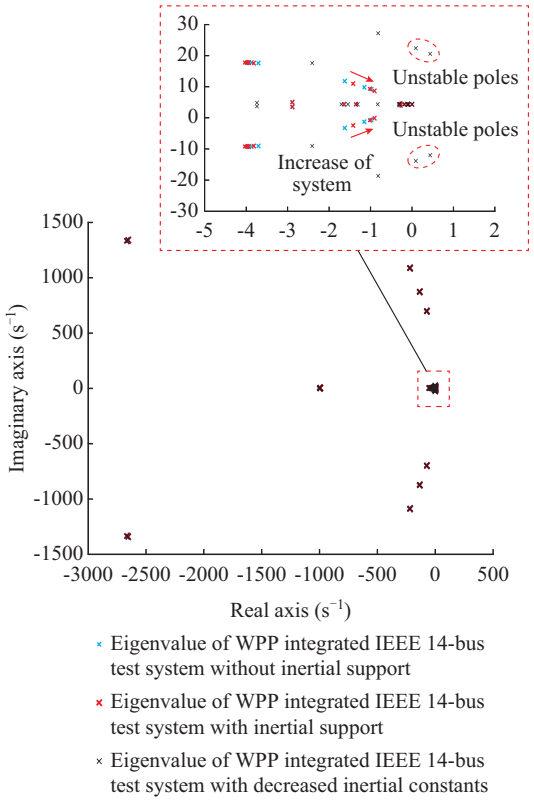

Fig. 11. Small-signal analysis at system level of WPP integrated IEEE 14-bus test system.

At high wind speed, the active power increment is limited for inertial controls. This is because the turbine is operated under the rated condition using pitch control before the disturbance. It is shown that the HSS speed is operated around 1600 r/min in Fig. 9(c). Compared with the baseline, the increased active power output (around 100 kW) is not significant due to the limited overproduction capability of WTG and power converters. Therefore, the improvement of FN is not as evident as the former two cases in which a large amount of turbine power is released during frequency response.

2) Mechanical Loadings in Turbine Shaft and Tower

The simulations in Fig. 10 reveal that the inertial controls can excite severe oscillations on the turbine shaft and tower. These oscillations are caused by turbine rotation in wind shears and relate to the lightly damped structural modes in flexible WTs. In low wind speed region of Fig. 10(a) and middle wind speed region of Fig. 10(b), it is clear that the coordinated TLIC with damping control can effectively suppress oscillations in LSS and tower in the side-to-side direction. The TLIC method with torque-rate limit holds the smallest magnitude of oscillations, but its inertial response is weakened accordingly as discussed in the previous sub-section. At the high wind speed as shown in Fig. 10(c), the loadings on LSS show less differences among the three compared algorithms, while the tower side-to-side bending shows a decreased trend with implemented inertial controls. It is obvious that at high wind speed, the proposed control can provide better damping on structural modes with reduced magnitude of oscillation on turbine tower and LSS. Compared with the other two scenarios, the inertial response without damping has smaller oscillation than the scenario with torque-rate limit. This is because the inertial response further reduces the aerodynamic power extraction from wind, resulting in a reduced aerodynamic force on turbine rotating plane. Such scenario is consistent with the previous research results in [21]. Note that the displacement on turbine tower will show periodic oscillations under steady state, which is induced by the rotation of turbine blades. The coordinate transformation [32] is usually required to convert the mechanical system model into a rotating reference frame, which is similar to the concept of Park transformation used in the analysis of electric machines.

C. Small-signal Analysis at Power System Level

In this part, the small-signal analysis at system level for WPP integrated IEEE 14-bus test system is conducted. The sub-section focuses on the interactions between WPP and the studied power system. Figure 11(a) gives the entire eigenvalue distribution of the system, and the zoomed-in eigenvalue distribution focusing on electro-mechanical dynamics of the system is shown in Fig. 11(b). The eigenvalues that are away from imaginary axis have fast natural oscillation frequencies, where corresponding transients can be damped out fast enough and the system stability concern will not be raised. As illustrated in Fig. 11(b), the participation of virtual inertial support from WPP (red case) is able to slightly drive the eigenvalues of the system toward right, so that the power system can obtain slower dynamics, and rate of change of frequency (ROCOF) is able to be mitigated. Compared with the blue case, the studied eigenvalues in red case have slightly higher damping ratio, which means its FN is able to be improved during frequency transient by integrating the proposed WT controller.

Unstable poles appear in the power system with reduced inertial constants, as the black case in Fig. 11(b), which further strengthens the importance of the proposed WTG inertial control method. By conducting small-signal analysis at system level, the interactions between multi-energy generation units can be comprehensively evaluated. The insights are provided on stability analysis of the system and design guidance on multi-energy systems. In fact, the frequency threshold of 59.8 Hz is ignored in this section in order to fully investigate the inertial control performance and eliminate the nonlinearity. Note that the eigenvalues with the slowest system dynamics are still maintained in the left-hand side of the complex plain. Meanwhile, no oscillatory behavior is introduced by these eigenvalues and they are not the poles of interest for inertial control analysis.

VI. Conclusion

In this paper, an enhanced WTG inertial control scheme with coordinated actions from supercapacitor ESS is proposed. High-fidelity models of the studied multi-energy system are presented using FAST for the mechanical sub-system. It has been proven that the proposed inertial control is able to provide effective power system frequency regulation without affecting the structural integrity of the WTG mechanical parts. The security of WTG system is considered and a feedback controller to damp structural modes in turbine shaft and tower is augmented by the modified TLIC method. ESS is mainly used to solve the SFD caused by KE restoration. The enhanced inertial response of multi-energy power system is studied through small-signal analysis at system level. Simulations show that the proposed method can improve the FN and mitigate SFD, and the magnitudes of oscillations in the mechanical subsystem decrease as well.

Appendix A

TABLE AI
Mechanical Parameters of CART3

Parameter	Value
Hub height	34.9 m
Hub radius	0.816 m
Drive-train torsional spring	2.47×10^7 N·m/rad
Drive-train torsional damper	1.4×10^4 N·m/s
Generator inertia	46 kg·m^2
Hub inertia	3899.7 kg·m^2
Nacelle inertia	36590 kg·m^2
Hub mass	6552 kg
Nacelle mass	23884.1 kg
Gearbox ratio	43.165
Maximum C_p	0.4658
Optimal TSR	7.1
Minimum pitch angle	3.7°
Rated rotor speed	41.7 r/min
MPPT control gain K_g	0.0813

Note: rotor radius is 20 m.

TABLE AII
Parameters of PMSG

Parameter	Value
Rated electric power	600 kW
Rated voltage	575 V
Rated rotor speed	1600 r/min
Number of pole pairs	1
Rated torque	3529.6 N·m
Torque limit	1.2 p.u.
Rotor flux linkage	2.1313 Wb
Stator resistance R_s	1.843 mΩ
d-axis stator inductance L_d	1.290 mH
q-axis stator inductance L_q	1.290 mH

Note: rated electric power is 600 kW.

TABLE AIII
Parameters of Power Converters

Parameter	Value
τ_{rsc} of current control loops	5 ms
τ_{gsc} of current control loops	1 ms
Rated DC voltage	3000 V
Resistance of RL filter	2.38 mΩ
Inductance of RL filter	200×10^{-3} mH

Note: the capacitance at DC link is increased to 1 Farad using the supercapacitor according to Section IV-C.

TABLE AIV
Key Parameters of IEEE 14-bus Test System

Generator	Capacity (MVA)	Inertial constant (s)	Generator voltage (kV)
SG1	615	7	22.0
SG2	100	5	13.8
SG3	180	6	13.8
SG4	120	5	13.8
SG5	60	4	13.8

References

[1] H. Jiang, Y. Zhang, J. Zhang *et al*., "PMU-aided voltage security assessment for a wind power plant," in *Proceedings of 2015 IEEE PES General Meeting*, Denver, USA, Aug. 2015, pp. 1-5.

[2] S. El Itani, U. D. Annakkage, and G. Joos, "Short-term frequency support utilizing inertial response of DFIG wind turbines," in *Proceedings of 2011 IEEE PES General Meeting*, Detroit, USA, Aug. 2011, pp. 1-8.

[3] Z. Wu, W. Gao, X. Wang *et al*., "Improved inertial control for permanent magnet synchronous generator wind turbine generators," *IET Renewable Power Generation*, vol. 10, no. 9, pp. 1366-1373, Oct. 2016.

[4] Y. Li, H. Zhang, X. Liang *et al*., "Event-triggered based distributed cooperative energy management for multienergy systems," *IEEE Transactions on Industrial Informatics*, vol. 15, no. 14, pp. 2008-2022, Apr. 2019.

[5] Y. Li, D. W. Gao, W. Gao *et al*., "Double-mode energy management for multi-energy system via distributed dynamic event-triggered newton-raphson algorithm," *IEEE Transactions on Smart Grid*, doi: 10.1109/TSG.2020.3005179.

[6] L. Qu and W. Qiao, "Constant power control of DFIG wind turbines with supercapacitor energy storage," *IEEE Transactions on Industry Applications*, vol. 47, no. 1, pp. 359-367, Jan.-Feb. 2011.

[7] F. D. Gonzalez, F. D. Bianchi, A. Sumper *et al*., "Control of a flywheel energy storage system for power smoothing in wind power plants," *IEEE Transactions on Energy Conversion*, vol. 29, no. 1, pp. 204-214, Mar. 2014.

[8] F. D. Gonzalez, A. Sumper, O. G. Bellmunt *et al*., "A review of energy storage technologies for wind power applications," *Renewable and Sustainable Energy Reviews*, vol. 16, no. 2012, pp. 2154-2171, Feb. 2012.

[9] Y. Li, Z. Xu, and K. P. Wong, "Advanced control strategies of PMSG-based wind turbines for system inertia support," *IEEE Transactions on Power Systems*, vol. 32, no. 4, pp. 3027-3037, Jul. 2017.

[10] J. Zhu, J. Hu, W. Hung *et al*., "Synthetic inertia control strategy for doubly fed induction generator wind turbine generators using lithium-ion supercapacitor," *IEEE Transactions on Energy Conversion*, vol. 33, no. 2, pp. 773-783, Jun. 2018.

[11] Z. Wu, D. Gao, H. Zhang *et al*., "Coordinated control strategy of battery energy storage system and PMSG-WTG to enhance system frequency regulation capability," *IEEE Transactions on Sustainable Energy*, vol. 8, no. 3, pp. 1330-1343, Jul. 2017.

[12] L. Miao, J. Wen, H. Xie *et al*., "Coordinated control strategy of wind turbine generator and energy storage equipment for frequency support," *IEEE Transactions on Industry Applications*, vol. 51, no. 4, pp. 2732-2742, Jul.-Aug. 2015.

[13] S. Zhang, Y. Mishra, and M. Shahidehpour, "Fuzzy-logic based fre-

quency controller for wind farms augmented with energy storage systems," *IEEE Transactions on Power Systems*, vol. 31, no. 2, pp. 1595-1603, Jan. 2016.
[14] J. Tan and Y. Zhang, "Coordinated control strategy of a battery energy storage system to support a wind power plant providing multi-timescale frequency ancillary services," *IEEE Transactions on Sustainable Energy*, vol. 8, no. 3, pp. 1140-1153, Mar. 2017.
[15] M. Kang, K. Kim, E. Muljadi *et al.*, "Frequency control support of a doubly-fed induction generator based on the torque limit," *IEEE Transactions on Power Systems*, vol. 31, no. 6, pp. 4575-4583, Nov. 2016.
[16] E. Muljadi, V. Gevorgian, and A. Hoke, "Short-term forecasting of inertial response from a wind power plant," in *Proceedings of 2016 IEEE Energy Conversion Congress and Exposition (ECCE)*, Milwaukee, USA, Sept. 2016, pp. 1-5.
[17] K. Jonson, L. Y. Pao, L. J. Fingersh *et al*., "Control of variable-speed wind turbines: standard and adaptive techniques for maximizing energy capture," *IEEE Control System*, vol. 26, no. 3, pp. 70-81, Jun. 2006.
[18] R. Fadaeinedjad, G. Moschopoulos, and M. Moallem, "The impact of tower shadow, yaw error, and wind shears on power quality in a wind-diesel system," *IEEE Transactions on Energy Conversion*, vol. 24, no. 1, pp. 102-111, Mar. 2009.
[19] R. Fadaeinedjad, M. Moallem, and G. Moschopoulos, "Simulation of a wind turbine with doubly fed induction generator by FAST and Simulink," *IEEE Transactions on Energy Conversion*, vol. 23, no. 2, pp. 690-700, Jun. 2008.
[20] P. Fleming, J. Aho, A. Buckspan *et al*., "Effects of power reserve control on wind turbine structural loading," *Wind Energy*, vol. 19, no. 3, pp. 453-469, Mar. 2015.
[21] X. Wang, W. Gao, A. Scholbrock *et al*., "Evaluation of different inertial control methods for variable-speed wind turbines simulated by FAST," *IET Renewable Power Generation*, vol. 11, no. 12, pp. 1534-1544, Oct. 2017.
[22] W. Yan, L. Cheng, S. Yan *et al*., "Enabling and evaluation of inertial control for PMSG-WTG using synchronverter with multiple virtual rotating masses in microgrid," *IEEE Transactions on Sustainable Energy*, vol. 11, no. 2, pp. 1078-1088, Apr. 2020.
[23] J. M. Jonkman and L. J. Buhl, "FAST user's guide," NREL, Golden, USA, Tech. Rep. Sept, 2005.
[24] A. D. Wright, "Modern control design for flexible wind turbines," NREL, Golden, USA, Tech. Rep. Jan, 2004.
[25] A. Yazdani and R. Iravani, *Voltage Sourced Converters in Power System: Modeling, Control and Applications*, New York: John Wiley & Sons, 2013.
[26] C. Abbey and G. Joos, "Supercapacitor energy storage for wind energy applications," *IEEE Transactions on Industry Applications*, vol. 43, no. 3, pp. 769-776, May-Jun., 2007.
[27] L. Qu and W. Qiao, "Constant power control of DFIG wind turbines with supercapacitor energy storage," *IEEE Transactions on Industry Applications*, vol. 47, no. 1, pp. 359-367, Jan.-Feb. 2011.
[28] S. Shah, P. Koralewicz, V. Gevorgian *et al*., "Large-signal impedance-based modeling and mitigation of resonance of converter-grid systems," *IEEE Transactions on Sustainable Energy*, vol. 10, no. 3, pp. 1439-1449, Jul. 2019.
[29] Y. Kim, M. Kang, E. Muljadi *et al*., "Power smoothing of a variable-speed wind turbine generator in association with the rotor-speed-dependent gain," *IEEE Transactions on Sustainable Energy*, vol. 8, no. 3, pp. 990-999, Jul. 2017.
[30] D. Yang, M. Kang, E. Muljadi *et al*., "Short-term frequency response of a DFIG-based wind turbine generator for rapid frequency stabilization," *Energies*, vol. 10, no. 11, pp. 1863-1876, Nov. 2017.
[31] B. J. Jonkman, L. Kilcher, "TurbSim user's guide," NREL, Golden, USA, Tech. Rep. Sept, 2012.
[32] G. Bir, "Multi-blade coordinate transformation and its application to wind turbine analysis," in *Proceedings of 46th AIAA Aerospace Sciences Meeting and Exhibit*, Reno, USA, Jan. 2008.

Weihang Yan received the B.S. degree and M.S. degree in control theory and engineering from School of Information Science and Engineering, Northeastern University, Shenyang, China, in 2014 and 2016, respectively. He is currently working toward the Ph.D. degree in electrical and computer engineering, University of Denver, USA. He also worked as a Research Intern with the NREL, Golden, USA. His research interests include dynamic modeling and control of renewable energy systems and stability analysis and control of microgrids.

Xiao Wang received the B.S. degree and Ph.D. degree in control theory and engineering from School of Information Science and Engineering, Northeastern University, Shenyang, China, in 2013 and 2018, respectively. During 2015 to 2017, he was a visiting Ph.D. student at the University of Denver, where he also worked as a student intern with the NREL, Golden, USA. He is currently with the Department of Electrical and Electronic Engineering, The University of Manchester, UK, as a Postdoctoral Research Associate. His research interests include stability and control of power systems related to renewable and storage integrations.

Wei Gao received the bachelor's degree in automation from Hebei University of Technology, Tianjin, China, in 2017. He is pursuing the Ph.D. degree in the Department of Electrical and Computer Engineering, University of Denver, Denver, USA. His research interests include microgrid control, renewable energy, and power system stability.

Vahan Gevorgian received the Ph.D. degree in electrical engineering from the State Engineering University of Armenia, Yerevan, Armenia, in 1993. He joined NREL in 1994 and has served many roles over the years. He is currently working with the Power Systems Engineering Center focused on renewable energy impacts on transmission and interconnection issues and dynamic modeling of variable generation systems. He provides technical support to NREL industry partners and major U.S. wind turbine manufacturers. He is member of the IEC Team for wind turbine power quality standards. His contributions to NREL research have been recognized through multiple Outstanding Individual and Team Staff awards. His research interests include dynamometer and field testing of large and small wind turbines, dynamometer testing of wind turbine drivetrain components, development of advanced data acquisition systems, and wind turbine power quality.